672–682 Nucleic Acids Research, 2010, Vol. 38, No. 2 Published online 11 November 2009
doi:10.1093/nar/gkp955

Two distinct regions in *Staphylococcus aureus* GatCAB guarantee accurate tRNA recognition

Akiyoshi Nakamura[1], Kelly Sheppard[2], Junji Yamane[1], Min Yao[1,3], Dieter Söll[2,4] and Isao Tanaka[1,3,*]

[1]Division of Biological Sciences, Graduate School of Science, Hokkaido University, Sapporo 060-0810, Japan, [2]Department of Molecular Biophysics and Biochemistry, Yale University, New Haven, CT 06520-8114, USA, [3]Faculty of Advanced Life Science, Hokkaido University, kita-10, nishi-8, Sapporo, Hokkaido, 060-0810, Japan and [4]Department of Chemistry, Yale University, New Haven, CT 06520-8114, USA

Received September 1, 2009; Revised October 6, 2009; Accepted October 10, 2009

ABSTRACT

In many prokaryotes the biosynthesis of the amide aminoacyl-tRNAs, Gln-tRNA^{Gln} and Asn-tRNA^{Asn}, proceeds by an indirect route in which mischarged Glu-tRNA^{Gln} or Asp-tRNA^{Asn} is amidated to the correct aminoacyl-tRNA catalyzed by a tRNA-dependent amidotransferase (AdT). Two types of AdTs exist: bacteria, archaea and organelles possess heterotrimeric GatCAB, while heterodimeric GatDE occurs exclusively in archaea. Bacterial GatCAB and GatDE recognize the first base pair of the acceptor stem and the D-loop of their tRNA substrates, while archaeal GatCAB recognizes the tertiary core of the tRNA, but not the first base pair. Here, we present the crystal structure of the full-length *Staphylococcus aureus* GatCAB. Its GatB tail domain possesses a conserved Lys rich motif that is situated close to the variable loop in a GatCAB:tRNA^{Gln} docking model. This motif is also conserved in the tail domain of archaeal GatCAB, suggesting this basic region may recognize the tRNA variable loop to discriminate Asp-tRNA^{Asn} from Asp-tRNA^{Asp} in archaea. Furthermore, we identified a 3_{10} turn in GatB that permits the bacterial GatCAB to distinguish a U1–A72 base pair from a G1–C72 pair; the absence of this element in archaeal GatCAB enables the latter enzyme to recognize aminoacyl-tRNAs with G1–C72 base pairs.

INTRODUCTION

Correct pairing of an amino acid with its cognate tRNA is an essential step to maintain the accuracy of translation. This is usually accomplished by aminoacyl-tRNA synthetases (aaRSs) that catalyze the direct attachment of an amino acid to its cognate tRNA (1). However, glutaminyl-tRNA synthetase (GlnRS) is absent in the majority of bacteria, in all known archaea, and in many organelles (2). These organisms utilize an indirect pathway for Gln-tRNA^{Gln} formation where a non-discriminating glutamyl-tRNA synthetase (ND-GluRS) synthesizes mischarged Glu-tRNA^{Gln} (3) that is then amidated to the cognate Gln-tRNA^{Gln} by glutamyl-tRNA^{Gln} amidotransferase (Glu-AdT) (2,4). Similarly, many prokaryotes lacking an asparaginyl-tRNA synthetase (AsnRS) generate Asn-tRNA^{Asn} by the combined actions of a non-discriminating aspartyl-tRNA synthetase (ND-AspRS) and an aspartyl-tRNA^{Asn} amidotransferase (Asp-AdT) (5,6).

Two types of AdTs exist: the heterotrimeric GatCAB (7) present in bacteria, archaea and organelles (2), and the heterodimeric GatDE found exclusively in archaea (8). GatDE specifically converts Glu-tRNA^{Gln} (8), while bacterial GatCAB acts as both a Glu-AdT and an Asp-AdT *in vitro* (2). The *in vivo* role of bacterial GatCAB is defined by the nature of ND-aaRS (ND-GluRS and/or ND-AspRS) present in the cell (2). In archaea that lack AsnRS, GatCAB is encoded (9). This enzyme (e.g. from *Methanothermobacter thermautotrophicus*) *in vitro* strongly prefers Asp-tRNA^{Asn} over the homologous Glu-tRNA^{Gln} (10); thus archaeal GatCAB may act *in vivo* as an Asp-AdT.

AdTs accurately distinguish their mischarged aa-tRNA substrates (Glu-tRNA^{Gln} and/or Asp-tRNA^{Asn}) from the cognate Glu-tRNA^{Glu} and Asp-tRNA^{Asp} species. Bacterial GatCAB and GatDE achieve this by recognizing the first base pair of the acceptor stem and the D-loop of their tRNA substrates (11–13). In contrast, archaeal GatCAB does not recognize the first base pair of Asp-tRNA^{Asn} (13,14). Instead the *M. thermautotrophicus* GatCAB makes use of the D-loop, the nucleotide in position 49, and to a lesser extent of the length of the variable loop to distinguish Asp-tRNA^{Asn} from

*To whom correspondence should be addressed. Tel/Fax: +81 11 706 3221; Email: tanaka@castor.sci.hokudai.ac.jp

Asp-tRNA^{Asp} (14), while the *Methanosarcina barkeri* GatCAB appears to use primarily the length of the variable loop for the same task (13).

Previous work implicated the tail domain of the GatB and GatE in D-loop recognition of their respective aa-tRNA substrates (11,12). These tail domains share homology with the standalone YqeY proteins of unknown function (PFAM id: PF09424) that are present in a diverse array of organisms (11,12,15,16). Previous crystallographic studies did not resolve the YqeY-like domain of AdTs (11,12,17,18) or of *Deinococcus radiodurans* GlnRS (15). Here, we present a full-length *Staphylococcus aureus* GatCAB structure (containing the YqeY domain) resolved at 1.9 Å. The structure reveals a Lys rich motif in the tail domain of GatB which is absent in GatE. We also identified by biochemical studies a bacterial GatCAB-specific element that enables this enzyme to distinguish a U1–A72 base pair from a G1–C72 pair.

MATERIALS AND METHODS

Preparation of *S. aureus* GatCAB

The enzyme was over-produced in an *Escherichia coli* B834 strain and purified over a HisTrap HP column (GE Healthcare) as described (11). The sample was then diluted 5-fold with Buffer *A* [50 mM Tris–HCl pH 7.5, 10 mM $MgCl_2$, 1 mM DTT and 10% (v/v) glycerol], and applied to a HiTrap Heparin HP column (GE Healthcare) equilibrated with buffer *A*. The column was washed with buffer *A* containing 50 mM NaCl, and proteins were eluted with a linear gradient of 50–500 mM NaCl. The enzyme eluted at ~250 mM NaCl. The enzyme fractions were then loaded onto a HiLoad 26/60 Superdex 200 pg column (GE Healthcare) equilibrated with buffer *B* [20 mM Tris–HCl pH 7.5, 10 mM $MgCl_2$, 1 mM DTT and 10% (v/v) glycerol]. Pooled fractions were concentrated by ultrafiltration using Vivaspin devices (VIVASCIENCE) to a final concentration of ~12 mg/ml. *S. aureus* GatCAB mutants were generated using the QuikChange™ site-directed mutagenesis kit according to the manufacture's protocol (Stratagene), and purified to homogeneity as described above.

Preparation of *M. thermautotrophicus* GatCAB and ND-AspRS

The over-production and purifications were as described (10). *Methanothermobacter thermautotrophicus* GatCAB mutants were generated as described above.

Preparation of *S. aureus* ND-GluRS

The gene encoding the ND-GluRS from *S. aureus* Mu50 was amplified by polymerase chain reaction (PCR). The *S. aureus* ND-GluRS is toxic for an *E. coli*, which does not possess GatCAB, therefore the gene was cloned into NcoI/XhoI site of a pTip vector, which is used to protein expression in *Rhodococcus erythropolis*, and then the *S. aureus* ND-GluRS protein was expressed in *R. erythropolis* as described (19). Cells were harvested (4000×*g*, 15 min at 4°C) and disrupted using sonication in buffer *C* [50 mM Tris–HCl pH 7.5, 300 mM NaCl, 5 mM $MgCl_2$, 10% (v/v) glycerol, 0.5 mg/ml lysozyme and 0.1 mg/ml DNase I]. All the following purification processes were carried out at 4°C. Cell debris was removed by centrifugation (40 000×*g*, 1 h), and clarified supernatant was applied to a HisTrap HP column as described (11). Pooled fractions were loaded onto a HiLoad 26/60 Superdex 200 pg column equilibrated with buffer *D* [20 mM HEPES-K pH 7.6, 5 mM $MgCl_2$, 100 mM KCl, 1 mM DTT and 10% (v/v) glycerol]. The purified *S. aureus* ND-GluRS was concentrated by ultrafiltration to a final concentration of 18 mg/ml, and then diluted 2-fold with 100% (v/v) glycerol, and stored at −30°C.

Preparation of *S. aureus* tRNA^{Gln}, and *M. thermautotrophicus* and *C. trachomatis* tRNA^{Asn}

The tRNA isoacceptors were *in vitro* transcribed and purified as described (10,11).

Preparation of aminoacyl-[^{32}P] labeled tRNA

The tRNA isoacceptors were [^{32}P]-labeled and aminoacylated as described (10,20) with minor modification. For glutamylation of *S. aureus* tRNA^{Gln}, 5 μM *S. aureus* ND-GluRS and tRNA^{Gln} were added in the aminoacylation reaction.

Crystallization and structure determination

The high quality single crystals of *S. aureus* GatCAB were obtained by using the micro-seeding technique (21) from hanging drops set up in a 1 : 1 : 0.1 ratio from protein, reservoir solution [25% (w/v) PEG 600, 5 mM $MgCl_2$, 50 mM HEPES–NaOH pH 7.2 and 3% (v/v) 2-methyl-2,4-pentanediol (MPD)] and a micro-seeds stock solution (21). The crystal of *S. aureus* GatCAB was rapidly soaked through the reservoir containing 50 mM MES-Na, pH 6.4, 25% (w/v) PEG 600, 5 mM $MgCl_2$, 3% (v/v) MPD and 10% (v/v) glycerol as a cryoprotectant, and then a data set was collected to 1.9 Å resolution at SPring-8 beamline 41XU (Hyogo, Japan) under cryogenic condition (−173°C). The data set was processed and scaled using the *HKL2000* package (22). The structure of *S. aureus* GatCAB was solved by molecular replacement using *AMoRe* in the CCP4 suite (23), with the refined model of the previous (11) *S. aureus* GatCAB structure (PDB ID: 2G5H) as a search model. The model of *S. aureus* GatCAB was rebuilt by automatic refinement program *LAFIRE* (24,25) running with *CNS* (26), and modified manually by using *Coot* (27) followed yielded the final model with the crystallographic R/R_{free} factor of 19.5/21.4%. The summary of data statistics is presented in Table 1. All figures were generated by *PyMol* (28).

Small-angle X-ray scattering

For preparation of the tRNA^{Gln}-bound *S. aureus* GatCAB, the *S. aureus* GatCAB was mixed with tRNA^{Gln} in a molar ratio of 1 : 4, and then purified by a

Table 1. Data collection and refinement statistics[a]

Data collection statistics	
PDB ID	3IP4
Beamline	SPring-8 BL41XU
Wavelength	1.00 Å
Space group	$P2_12_12_1$
Cell dimensions *a*, *b*, *c* (Å)	71.1, 92.7, 180.4
Resolution (Å)	50.00–1.90 (1.97–1.90)
R_{merge}[b]	0.070 (0.457)
$I/\sigma(I)$	23.2 (3.5)
Completeness (%)	99.9 (100)
Redundancy	7.0
Refinement statistics	
Resolution (Å)	20.0–1.90
No. reflections	94598
R_{work}[c]/R_{free}[d]	0.195/0.214
Number of atoms (protein/water/others)	8299/801/1
Average B factors (Å^2) (protein/water/others)	33.6/35.3/26.0
RMSD bond length (Å)/angles (°)	0.006/1.3
Ramachandran plot (%)	
Favored	90.2
Allowed	9.6
Generous	0.2

[a]Values in parentheses are for the outermost resolution shell.
[b]$R_{merge} = \Sigma_h\Sigma_j|<I>_h - I_{h,j}|/\Sigma_h\Sigma_j I_{h,j}$, where $<I>_h$ is the mean intensity of symmetry-equivalent reflections.
[c]$R_{work} = \Sigma||F_{obs}| - |F_{cal}||/\Sigma|F_{obs}|$, where F_{obs} and F_{cal} are observed and calculated structure factor amplitudes.
[d]R_{free} value was calculated for *R* factor, using only an unrefined subset of reflections data.

gel filtration using a Superdex 200 10/300 GL column (GE Healthcare) in buffer *B*.

Small-angle X-ray scattering (SAXS) measurements were carried out at SPring-8 beamline 40B2 and 45XU (Hyogo, Japan) (29). The following SAXS analysis was carried out by using the data measured at BL45XU. A wavelength of 1.0 Å was used, and the specimen-to-detector distance was 246.5 cm. The scattering vector range was $0.008\,Å^{-1} < s < 0.334\,Å^{-1}$, where $s = 4\pi\sin\theta/\lambda$, with 2θ being the scattering angle. Data were measured at 5.0 mg/ml of samples at 25°C. Both buffers and samples were exposed 100 s. The SAXS data were normalized to the intensity of the incident beam and processed to background subtraction using the standard procedures with the program package *PRIMUS* (30). Maximum particle dimensions D_{max} were computed using the indirect transform package *GNOM* (31), which also gives the distance distribution functions $p(r)$. The discrepancy between the calculated and the experimental scattering curves was minimized using the program *CRYSOL* (32) as described previously (33,34). The 16 *ab initio* models of tRNA-free and -bound *S. aureus* GatCAB were generated and averaged with the program *DAMMIN* (35), *DAMAVER* (36) and *SUPCOMB* (37) as described previously (34).

[^{32}P]tRNA/nuclease P1 amidotransferase assay

AdT activities of wild-type and mutant GatCAB enzymes were monitored using a [^{32}P]tRNA/nuclease P1 amidotransferase assay as previously described (38). Determination of kinetic parameters with the *S. aureus* GatCAB enzymes was carried out as described for the *Helicobacter pylori* GatCAB (20). Determination of the kinetic parameters with the *M. thermautotrophicus* GatCAB enzymes was carried out as described (10).

RESULTS

Overall structure of a full-length GatCAB

We crystallized *S. aureus* GatCAB by adding 3–10% (v/v) MPD to the previous crystallization condition (11), which dramatically improved the crystal quality (maximum resolution from 2.3 to 1.9 Å). Surprisingly, the high-resolution structure clearly shows the GatB C-terminal region encompassing amino acids 412–475 and a histidine-tag (Figure 1A and Supplementary Figure S1), whose electron density map was not visible in the previous crystal structures. Although the unit cell dimension and crystal packing of the full-length and the previous apo-form *S. aureus* GatCAB are very similar, in the current structure the C-terminal GatB region is sandwiched between two GatA molecules related by 2-fold screw axes. Successful resolution of the tail-domain may be due to MPD addition in the crystallization mixture making the protein domain less flexible.

The GatA apo-form is essentially the same as the previously deposited *S. aureus* GatA structures (11). Interestingly, the high-resolution structure shows an alternative conformation for R358, which recognizes the carboxyl group of the substrate Gln (Supplementary Figure S2). Furthermore, Y310, which made a hydrogen bond with D425 in the Gln-bound *S. aureus* GatCAB (PDB ID: 2F2A), is flipped out from the active site of GatA, indicating that Gln binding induces only minor conformational changes in the GatA active site. GatC is also nearly identical to the deposited *S. aureus* GatC structures except the six C-terminal residues (95–100) were disordered and could not be modeled.

GatB is comprised of three consecutive domains: a cradle domain (1–294), a helical domain (295–407) and a tail domain (412–475). The cradle and helical domains are identical to the *S. aureus* GatB apo-form (PDB ID: 2G5I), and the permanent Mg^{2+} in the catalytic pocket was visible (11,18). The tail domain forms an anti-parallel helix bundle with three amphiphilic helices (α13, α15 and α16) that construct a hydrophobic core with α14 (Figure 1B and Supplementary Figure S1). L472 participates in this hydrophobic core and is not exposed to the molecular surface, indicating L472 is important for maintaining the structure of the tail domain rather than directly recognizing the aa-tRNA substrate as previously suggested (11). The loop between α15 and α16 interacts with I412 and S413 by two main chain and one side chain hydrogen bonds. Therefore, the *S. aureus* GatB tail and helical domains are linked by a ~13 Å long inter-domain loop (408–411).

Comparison of the GatB tail domain with YqeY

The C-terminal end of GatB, comprised of the helical and tail domains (295–475), belongs to the same protein family

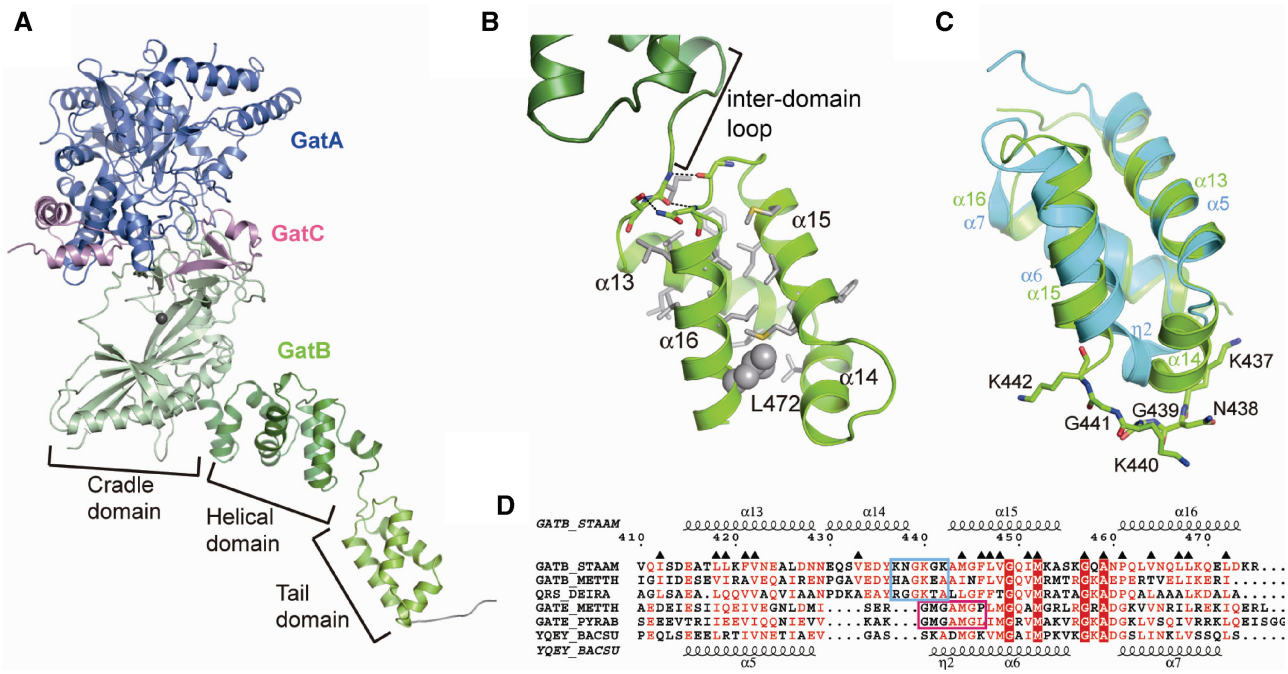

Figure 1. (**A**) Overall structure of the full-length GatCAB. GatA and GatC are colored blue and magenta, respectively. GatB contains three domains: the cradle, the helical and the tail domain (light green, dark green and yellow green, respectively). Mg atom (black) in the cradle domain and C-terminal His-tag (grey) are also shown. (**B**) The structure of the GatB tail domain. The residues involved in the hydrophobic core are shown as a grey stick model, along with hydrogen bonds between the inter-domain loop and the tail domain (indicated as dashed lines). L472 is indicated as a grey sphere model. (**C**) Superposition of the *S. aureus* tail domain (yellow green) and YqeY-C (cyan), where the Lys rich motif is indicated as a stick model. (**D**) Structural based sequence alignments of the tail domain of YqeY-like proteins. Secondary structure of *S. aureus* tail domain is indicated at top, and that of YqeY-C is indicated at bottom (α, α-helix; β, β-strand; η, 3_{10}- turn). The number at top is corresponding to *S. aureus* GatB sequence. The residues constructing the hydrophobic core of *S. aureus* tail domain are marked with filled triangles. The Lys rich motif and the GXXAXGX motif are shown as cyan box and magenta box, respectively. The species aligned are as follows: STAAM *S. aureus*, METTH, *M. thermautotrophicus*; DEIRA, *D. radiodurans*; PYRAB, *P. abyssi*; BACSU, *B. subtilis*.

as standalone YqeY polypeptides of unknown function present in many bacteria and in yeast (PFAM ID: PF09424) (15,16). The YqeY-like tail domain appended to the *D. radiodurans* GlnRS enables the enzyme to productively bind to $tRNA^{Gln}$ (15). A similar role is proposed for this structure in GatB and GatE via recognition of the D-loop (11,12). The only YqeY structure so far resolved is from *Bacillus subtilis* (PDB ID: 1NG6); it can now be compared with the YqeY region in the present full-length of *S. aureus* GatCAB structure. The anti-parallel helix bundle of the tail domain superimposes well with the C-terminal domain of *B. subtilis* YqeY protein (YqeY-C: 92-146) with an *r.m.s.* deviation of 1.97 Å for the 51 Cα pairs compared (Figure 1C). Interestingly, the GatB tail domain has an additional α-helix (α14) and a short loop between α14 and α15 (439–442) not found in the YqeY-C. Based on the multiple sequence alignment with the tail domains and YqeY-C, this extended region contains a Lys rich motif (KXGKXK) that is highly conserved in bacterial and archaeal GatB enzymes (Figure 1D and Supplementary Figure S3). The C-terminal extension of *D. radiodurans* GlnRS also contains this extended region with a similar motif (RGGKTA). In contrast to GatB and *D. radiodurans* GlnRS, the tail domain of GatE lacks α14 and the Lys rich motif. Interestingly, the Lys rich motif of GatB is instead replaced in GatE with a GXXAXGX motif that has been implicated in GatDE distinguishing Glu-$tRNA^{Gln}$ from Asp-$tRNA^{Asn}$ (16).

Docking $tRNA^{Gln}$ into the *S. aureus* GatCAB structure

The GatB C-terminal tail is essential for GatCAB binding $tRNA^{Gln}$ (11). In the co-crystal structure of the GatDE enzyme (PDB ID: 2D6F), the GatE tail domain was in the vicinity of the tRNA D-loop; however, its detailed structure could not be solved and the D-loop was fitted with the help of the *B. subtilis* YqeY-C structure (12). We decided to create a docking model of full-length *S. aureus* GatCAB with *E. coli* $tRNA^{Gln}$ to understand how the enzyme uses the tail domain to bind the tRNA. The use of *E. coli* $tRNA^{Gln}$ is reasonable as the sequences of the variable and D-loops of the *S. aureus* and *E. coli* $tRNA^{Gln}$ are identical (Figure 2A), and *E. coli* Glu-$tRNA^{Gln}$ serves as substrate for GatCAB *in vivo* (39).

To construct the docking model we first superposed *E. coli* $tRNA^{Gln}$ (PDB ID: 1QTQ) into the GatDE:$tRNA^{Gln}$ co-crystal structure by aligning all atoms of nucleotides U8, A14–G19, A21, C48 and U54–G57 of the tRNAs. The U8–A14–A21 base triple in the augmented D-stem is commonly found in $tRNA^{Gln}$ while nucleotide 15 in the D-loop and nucleotide 48 in the variable loop form the conserved Levitt pair (40,41).

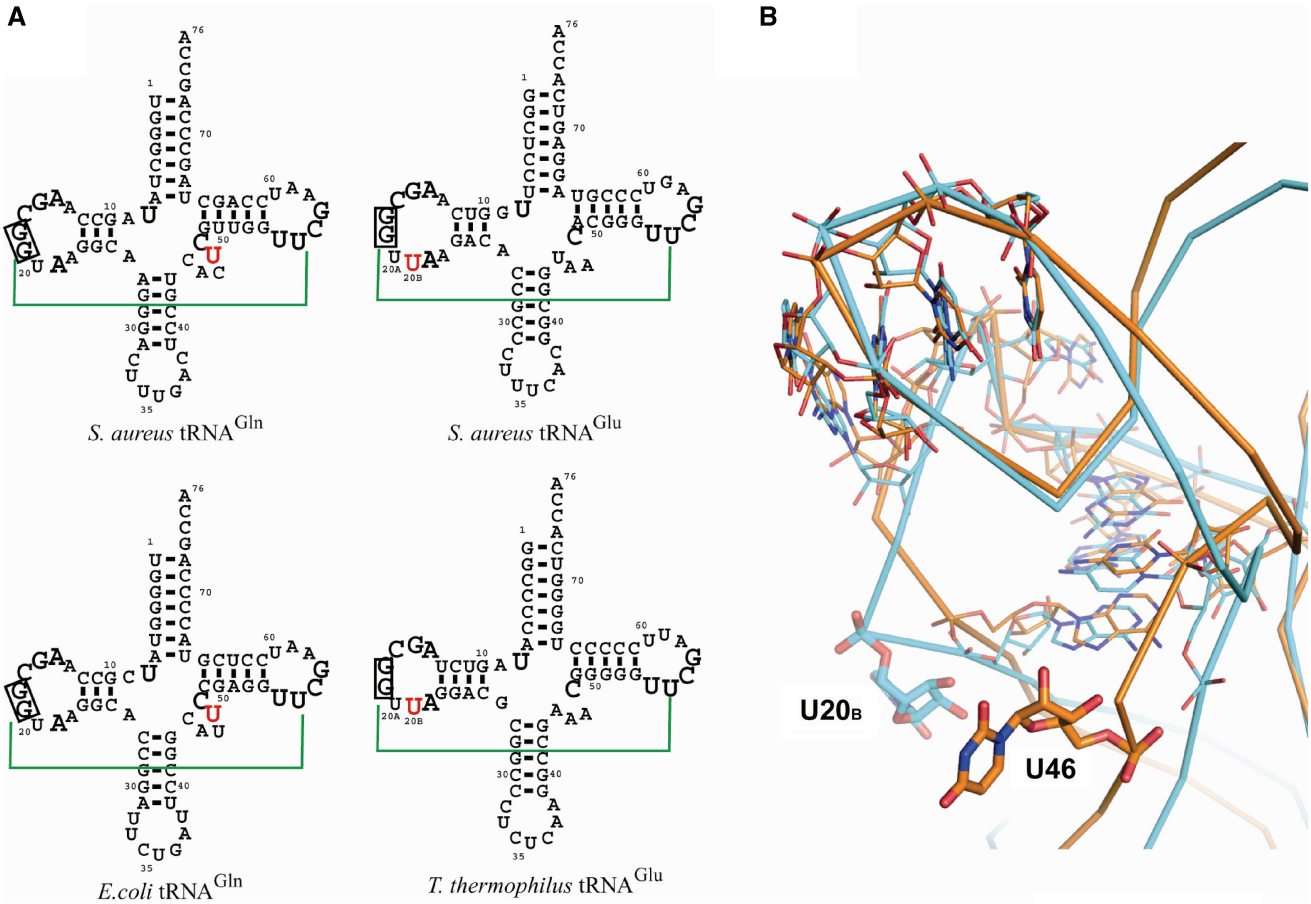

Figure 2. Comparison with $tRNA^{Gln}$ and $tRNA^{Glu}$. (**A**) Secondary structures of $tRNA^{Gln}$ $tRNA^{Glu}$ from *S. aureus*, *E. coli* and *T. thermophilus*. The G18:C56 base pair are colored green. The two guanines conserved in the tRNA D-loop are enclosed with black boxes. U8, A14–G19, A21, C48 and U54–G57, which employed on superposing of $tRNA^{Gln}$ and $tRNA^{Glu}$, are shown as black large characters. U47 of $tRNA^{Gln}$ and $U20_B$ of $tRNA^{Glu}$ are colored red. (**B**) Superposition of the *E. coli* $tRNA^{Gln}$ and *T. thermophilus* $tRNA^{Glu}$. Orange and cyan ribbon diagram indicate *E. coli* $tRNA^{Gln}$ and *T. thermophilus* $tRNA^{Glu}$, respectively. Supplemental nucleotides of the variable loop of *E. coli* $tRNA^{Gln}$ and the D-loop of *T. thermophilus* $tRNA^{Glu}$ are shown as thick stick models. The U8–A14–A21 base-triple, the conserved 'Levitt' pair and tRNA D-loop and TΨC -loop associating nucleotides are indicated as thin stick models.

The tertiary interaction between the D- and TΨC- loops of tRNA is also well conserved.

Next, we docked *S. aureus* GatCAB to $tRNA^{Gln}$ by taking advantage of the homology between GatB and GatE (8,16), and the co-crystal structure of GatDE:$tRNA^{Gln}$ (12), superposing GatB with *M. thermautotrophicus* GatE. The cradle domain of *S. aureus* GatB and *M. thermautotrophicus* GatE superpose well with an r.m.s. deviation of 1.7 Å for 244 pairs of Cα atoms compared. However, initially there were severe clashes between the helical domain and $tRNA^{Gln}$. Therefore, we separated the helical and tail domains into three parts (293–363, 364–381 and 382–475) and then superposed into GatE independently. Such movements are predicted based on previous AdT structures (11,12,17). Finally, the cradle and helical domains of *S. aureus* GatB could be superposed into that of *M. thermautotrophicus* GatE with an r.m.s. deviation of 1.9 Å for 321 pairs of Cα atoms compared (Supplementary Figure S4A).

The GatB tail domain possesses a highly conserved hydrophobic pocket comprised by residues (V449, M452, G457, A459 and P461) from the α15, α16 and the loop between them (Figure 3A), surrounded by positively charged residues (Figure 3B). In contrast, the opposite surface of the tail domain is composed of non-conserved, mostly negative residues (Figure 3A and B). These observations suggest that this conserved hydrophobic pocket may recognize the shape of the $tRNA^{Gln}$ D-loop with the surrounding positive residues interacting with the tRNA phosphate backbone (Figure 3C).

Interaction of the tail domain with tRNA is expected, as deletion of the C-terminal portion of GatB gives rise to a GatCAB mutant enzyme unable to bind tRNA (11) and as mentioned the electron density map of the GatDE:$tRNA^{Gln}$ structure places the YeqY-like tail domain in proximity of the tRNA D-loop (12). However, the initial *S. aureus* GatCAB:$tRNA^{Gln}$ docking model placed the conserved hydrophobic pocket of the tail domain ~12 Å away from the D-loop of $tRNA^{Gln}$ (Supplementary Figure S4B). It is likely that the tail domain can move to interact with $tRNA^{Gln}$ due to the flexible loop connecting the tail and helical domains. This domain flexibility may explain why it has

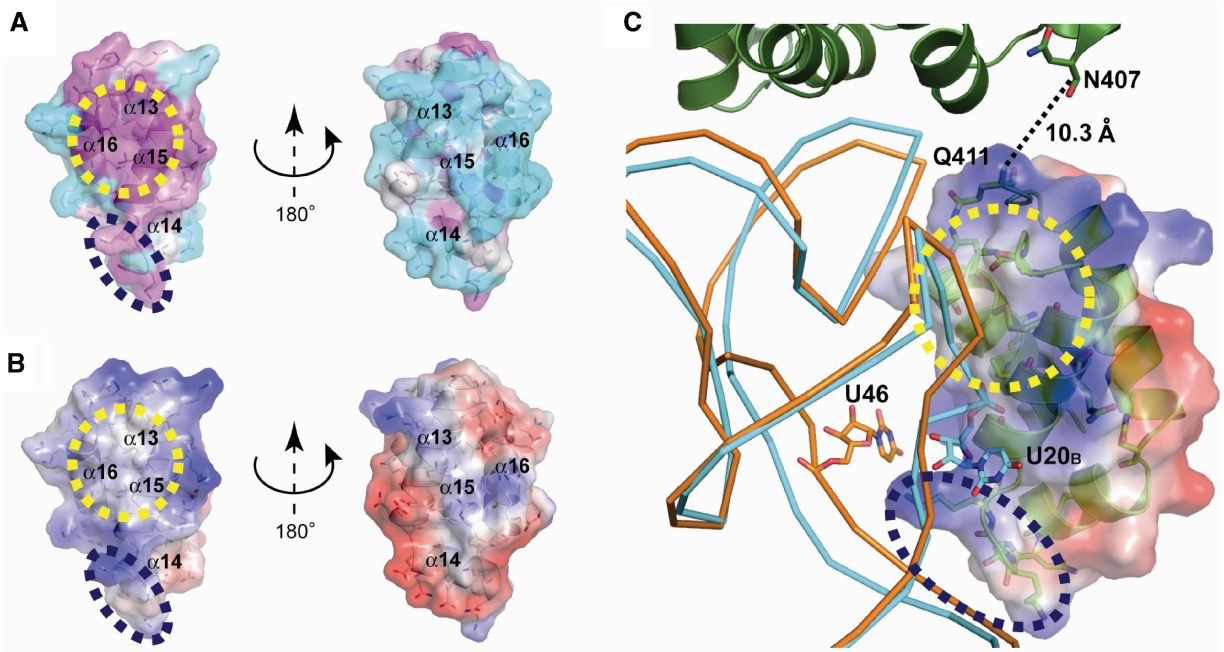

Figure 3. (**A**) Surface representation with a ribbon diagram of *S. aureus* tail domain is shown, and is colored by the sequence conservation among bacterial GatB using the program *ConSurf 3.0*: from low to high (cyan to white to magenta). The conserved hydrophobic pocket and the Lys rich motif are shown as yellow and purple dashed circles, respectively. (**B**) Solvent-accessible surface with a ribbon diagram of *S. aureus* tail domain is shown in the same orientation as (A) and is colored according to the electrostatic potential calculated by the program *APBS* running on *Pymol* (blue for positively charged and red for negatively charged). (**C**) The *S. aureus* tail domain docking model. *S. aureus* tail domain is shown as in (B). Orange and cyan ribbon diagram indicate *E. coli* $tRNA^{Gln}$ and *T. thermophilus* $tRNA^{Glu}$, respectively. Supplemental nucleotides of the variable loop of *E. coli* $tRNA^{Gln}$ and the D-loop of *T. thermophilus* $tRNA^{Glu}$ are shown as a stick model. The helical domain from the *S. aureus* GatB:$tRNA^{Gln}$ docking model (described below) shown together. The inter-domain loop between the helical and the tail domain is shown as dashed lines.

been difficult to resolve the YqeY-like tail of previous AdT structures (11,12,17,18). Given the above, we manually fitted the pocket of the tail domain into the D-loop of the *E. coli* $tRNA^{Gln}$ (Figure 3C). The distance between the N-terminal end of the tail domain (Q411) and the C-terminal end of the helical domain (N407) is ~10 Å, a distance the inter-domain loop connecting the two domains can bridge (Figure 3C). Recognition of the D-loop is consistent with the fact bacterial GatCAB uses that tRNA element to distinguish transamidation substrates (Glu-$tRNA^{Gln}$ and Asp-$tRNA^{Asn}$) from Glu-$tRNA^{Glu}$ and Asp-$tRNA^{Asp}$ (11,13).

In order to verify our final *S. aureus* GatB:$tRNA^{Gln}$ docking model, we recorded small-angle X-ray diffusion spectra on the tRNA-free and -bound *S. aureus* GatCAB purified by a size exclusion chromatography (Supplementary Figure S5). The predicted curve calculated from the crystal structure of the full-length *S. aureus* GatCAB with the program *CRYSOL* (32) fits closely to the experimental curve of tRNA-free *S. aureus* GatCAB, as characterized by a discrepancy value χ of 0.050 (Figure 4A). Furthermore, the crystal structure fits well to the *ab initio* envelope calculated with the program *DAMAVER* (36), of 16 dummy atom models calculated with *DAMMIN* (35), as reflected by a normalized spatial discrepancy (NSD) value of 1.21 (4A). The predicted scattering curve of the $tRNA^{Gln}$ docking model fits well the experimental curve of tRNA-bound *S. aureus* GatCAB (χ of 0.098) and the *ab initio* envelope (NSD of 0.97) (Figure 4A). However, the $tRNA^{Gln}$ docking model before fitting the tail domain shows a significantly higher discrepancy value with the experimental curve of tRNA-bound *S. aureus* GatCAB and the *ab initio* envelope (χ of 0.186 and NSD of 1.08, respectively) than using the tail domain fitting model. These results suggest that our docking model with the tail domain interacting with the tRNA is consistent with the solution structure of the *S. aureus* GatCAB:$tRNA^{Gln}$ complex.

In our docking model, the hydrophobic pocket of the GatB tail domain nicely accommodates the curve of the $tRNA^{Gln}$ D-loop (Figure 3C). The *S. aureus* enzyme distinguishes $tRNA^{Gln}$ from $tRNA^{Glu}$ based on the presence of an extra base ($U20_B$) in the D-loop of $tRNA^{Glu}$ (11). To gain a better understanding of how this is accomplished we superposed the structures of *E. coli* $tRNA^{Gln}$ (PDB ID: 1QTQ) and *Thermus thermophilus* $tRNA^{Glu}$ (PDB ID: 1G59) in a similar manner as described above. The D-loop of *T. thermophilus* $tRNA^{Glu}$ like that of *S. aureus* $tRNA^{Glu}$ possesses a $U20_B$ supernumerary base (Figure 2A). That extra base flips out from the tRNA D-loop and TΨC-loop associating region (Figure 2B). In the docking model of the tail domain with tRNA, the flipped out $U20_B$ in the D-loop of $tRNA^{Glu}$ could not be accommodated; the extra base sterically clashes with the surface of the protein in the model (Figure 3C), suggesting that is the mechanism by which *S. aureus* GatCAB rejects $tRNA^{Glu}$.

In addition to recognition of the D-loop, the GatB tail domain may also bind to the variable loop of the tRNA. In our docking model, the GatB-specific Lys rich motif of

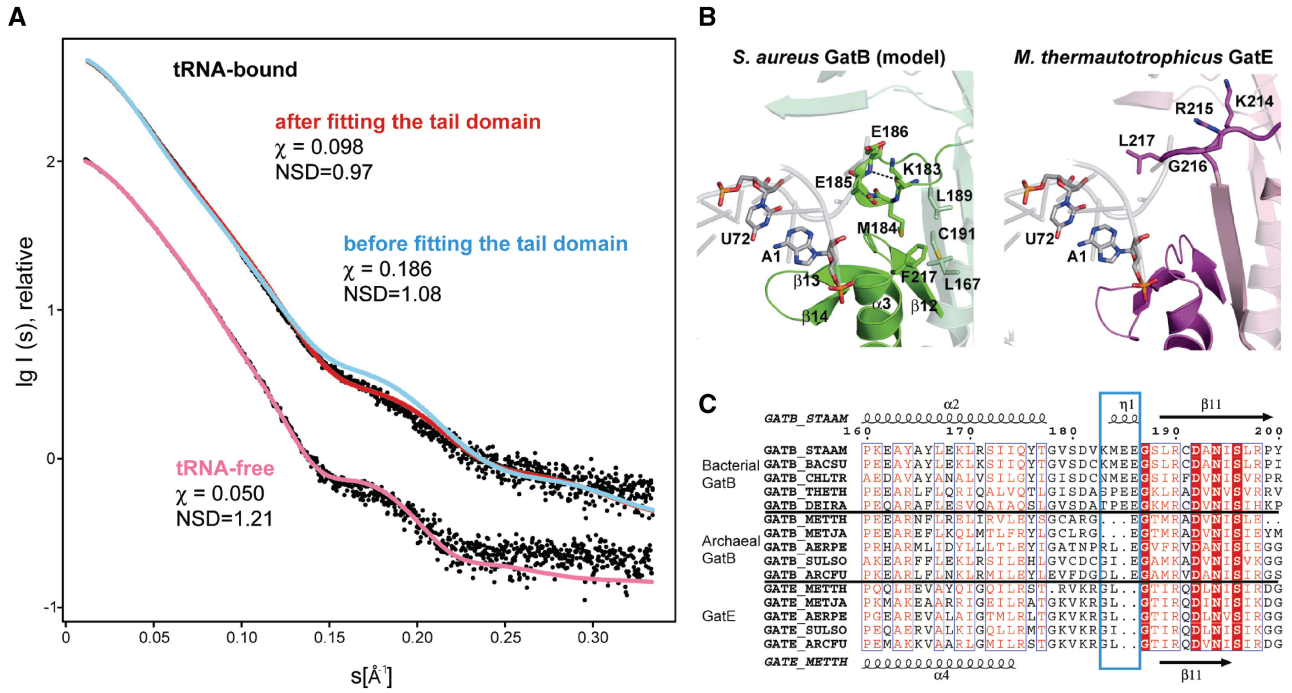

Figure 4. (**A**) Experimental and computed SAXS scattering data. (Upper) the tRNA-bound GatCAB, (lower) tRNA-free GatCAB. The logarithm of the scattering intensity is plotted against the momentum transfer $s = 4\pi\sin\theta/\lambda$, where 2θ is the scattering angle and $\lambda = 1.0$ Å is the X-ray wavelength. The plots are displaced along the ordinate for better visualization. Red, cyan and pink curves indicated the computed scattering from tRNA-bound GatCAB model after the tail domain fitting, before the tail domain fitting, and tRNA-free GatCAB, respectively. (**B**) Comparison of the model of the *S. aureus* GatB:tRNA^{Gln} complex (left) and the crystal structure of the *M. thermautotrophicus* GatE:tRNA^{Gln} complex (right). *S. aureus* GatB, *M. thermautotrophicus* GatE *and M. thermautotrophicus* tRNA^{Gln} are shown as green, magenta and grey ribbon diagram, respectively. The A1–U72 base pair of *M. thermautotrophicus* tRNA^{Gln} is shown as a stick model. The 3_{10} turn and the hydrophobic core of *S. aureus* GatB and the short loop of *M. thermautotrophicus* GatE are also shown. (**C**) Structural based sequence alignments of the cradle domain of bacterial GatB, archaeal GatB and GatE. The number at top is corresponding to *S. aureus* GatB sequence. Secondary structure of *S. aureus* GatB is indicated at top, and that of *M. thermautotrophicus* GatE is indicated at bottom. The 3_{10} turn of bacterial GatB and the corresponding region of archaeal GatB and GatE are shown as cyan box. The species aligned are as follows: CHLTR, *Chlamydia trachomatis*; THETH, *Thermus thermophilus HB8*; METJA, *Methanococcus jannaschii*; AERPE, *Aeropyrum pernix*; SULSO, *Sulfolobus solfataricus*; ARCFU, *Archaeoglobus fulgidus*.

the tail domain is situated in proximity to the variable loop of tRNA^{Gln}, in particular U46 which is pushed out from the tertiary core of the tRNA (Figures 2B and 3C). Consistent with this prediction, replacement of this Lys rich motif with the GXXAXGX motif from GatE results in a mutant *S. aureus* GatCAB enzyme with reduced affinity for tRNA (Supplementary Figure S6).

The GatB cradle domain recognizes the first base pair of the acceptor stem

Bacterial GatCAB enzymes recognize the U1–A72 base pair of the acceptor stem of Glu-tRNA^{Gln} and Asp-tRNA^{Asn} to discriminate them from Glu-tRNA^{Glu} and Asp-tRNA^{Asp} (11,13). In contrast, archaeal GatCAB does not use the first base pair of the tRNA acceptor stem to distinguish Asp-tRNA^{Asn} from Asp-tRNA^{Asp}, recognizing aa-tRNA species with either a U1–A72 or a G1–C72 base pair (10,13,14). However, the process of distinguishing a U1–A72 base pair from a G1–C72 base pair is not known.

In our GatCAB:tRNA^{Gln} docking model the tRNA^{Gln} acceptor stem U1–A72 base pair is located in the center of the cradle domain in a space constructed by α3, two internal loops between β12–α3 and β13–β14, and a 3_{10} turn between α2–β11. The 3_{10} turn is adjacent to the U1–A72 base pair (Figure 4B). This 3_{10} turn is constructed by a hydrogen bond between the main-chain carbonyl oxygen of K183 and amide of E186. Furthermore, M184 in the 3_{10} turn forms a hydrophobic core with L167, L189, C191 and F217, suggesting the 3_{10} turn is fixed with α3 and β11 by a hydrophobic interaction. In the GatDE enzyme, GatE has a short loop in place of a 3_{10} turn at the corresponding region (Figure 4B and C).

In an alignment of GatB and GatE sequences (Figure 4C), the region including the 3_{10} turn (183–186 in *S. aureus* GatB) is conserved in bacterial GatB sequences, and the corresponding region in archaeal GatB is 1–3 residues shorter, suggesting archaeal GatB has a loop in place of the 3_{10} turn like GatE. The loop region of GatE is well conserved and is rich in positive residues, however the corresponding region in archaeal GatB is not well conserved. The docking model and alignment suggest these structural differences between bacterial GatB, archaeal GatB and GatE may enable the differences in first base pair recognition between the enzymes. In particular, they imply that the 3_{10} turn enables bacterial GatB to distinguish a U1–A72 from a G1–C72 base pair.

Table 2. Transamidase activity of the *S. aureus* (*Sa*) GatCAB and *M. thermautotrophicus* (*Mt*) GatCAB with different mischarged tRNA substrates

aa-tRNA[a]	Transamidase activity (s^{-1})			
	Sa GatCAB[b]		*Mt* GatCAB[b]	
	wt	$3_{10}\Delta$	wt	$3_{10\ ins}$
Sa Glu-tRNA$^{Gln}_{UA}$	0.71 ± 0.03	0.05 ± <0.01	0.0035 ± 0.0003	0.0047 ± 0.0002
Sa Glu-tRNA$^{Gln}_{GC}$	0.05 ± <0.01	0.03 ± <0.01	0.0014 ± 0.0002	0.0004 ± 0.0002
Mt Asp-tRNA$^{Asn}_{GC}$	0.05 ± 0.03	0.04 ± 0.01	0.05 ± 0.01	0.01 ± <0.01
Ct Asp-tRNA$^{Asn}_{UA}$	0.24 ± <0.01	0.02 ± <0.01	0.04 ± <0.01	0.11 ± <0.01

Measurements were from three separate experiments. Standard deviations are reported. Reactions were carried out at 37°C in the presence of ATP (4 mM), amide donor (4 mM) and aa-tRNA (1.25 μM) indicated.
[a]The aa-tRNA substrates tested were the *S. aureus (Sa)* wild-type Glu-tRNA$^{Gln}_{UA}$ and mutant Glu-tRNA$^{Gln}_{GC}$, the wild type of the *M. thermautotrophicus (Mt)* Asp-tRNA$^{Asn}_{GC}$ and the *C. trachomatis* (*Ct*) Asp-tRNA$^{Asn}_{UA}$.
[b]In the reactions, concentrations of the GatCAB indicated [*Sa* wild-type (wt) GatCAB, *Sa* 3_{10} turn deleted mutant GatCAB ($3_{10}\Delta$), *Mt* wt GatCAB, or *Mt* 3_{10} turn insertion mutant GatCAB ($3_{10\ ins}$)] ranged from 20 nM to 1 μM.

Table 3. Kinetic data for the transamidase activity of the *S. aureus* and *M. thermautotrophicus* GatCAB mutants with different mischarged tRNA substrates

Enzyme	*Sa* Glu-tRNA$^{Gln}_{UA}$			*Mt* Asp-tRNA$^{Asn}_{GC}$			*L*
	K_M (mM)	k_{cat} (s^{-1})	k_{cat}/K_M (s^{-1}/mM)	K_M (mM)	k_{cat} (s^{-1})	k_{cat}/K_M (s^{-1}/mM)	
Sa wt	1.80 ± 0.22	1.7 ± 0.1	930 ± 120	2.05 ± 0.48	0.1 ± <0.1	60 ± 15	15.5
Sa $3_{10}\Delta$	1.85 ± 0.59	0.1 ± <0.1	54 ± 18	0.61 ± 0.40	0.04 ± <0.01	67 ± 44	0.8
Mt wt	0.70 ± 0.26	0.006 ± 0.001	8 ± 3	0.78 ± 0.30	0.10 ± 0.01	125 ± 49	15.6
Mt $3_{10\,ins}$	0.97 ± 0.22	0.009 ± 0.001	9 ± 2	2.51 ± 0.51	0.03 ± <0.01	12 ± 3	1.3

Measurements were from three separate experiments. Standard deviations are reported. Reactions were carried out at 37°C in the presence of excess ATP (4 mM) and Gln (4 mM). *L* is the relative catalytic efficiency [(k_{cat}/K_M of homologous substrate)/(k_{cat}/K_M of non-homologous substrate)]. GatCAB enzymes labeled like in Table 2.

The 3_{10} turn of bacterial GatB is crucial for tRNA^{Gln} acceptor helix U1–A72 base pair recognition

To evaluate the relation between the presence of the 3_{10} turn in GatB and the specificity of first base pair recognition, we constructed a mutant *S. aureus* GatCAB enzyme in which the 3_{10} turn (K183, M184 and E185) is replaced by the short putative loop from *M. thermautotrophicus* GatB. Based on the multiple sequence alignment (Figure 4C) we also constructed a mutant *M. thermautotrophicus* GatCAB where the 3_{10} turn (residues Lys, Met and Glu) is inserted into GatB between residues Gly169 and Glu170. We then tested the transamidase activities (Tables 2 and 3) by the [^{32}P]tRNA/nuclease P1 assay (38) of these mutant GatCAB enzymes with a variety of tRNA substrates.

As expected (10,13,14), wild-type *S. aureus* GatCAB prefers tRNAs with a U1–A72 base pair over those with a G1–C72 base pair, while wild-type *M. thermautotrophicus* GatCAB has no strong preference (Table 2). *S. aureus* Glu-tRNA^{Gln} was a poor substrate for wild-type *M. thermautotrophicus* GatCAB (Tables 2 and 3), like *B. subtilis* Glu-tRNA^{Gln} for unknown reasons (10). However, the transamidase activity of wild-type *M. thermautotrophicus* GatCAB with wild-type Glu-tRNA^{Gln} containing a U1–A72 base pair was approximately the same as with the G1–C72 mutant Glu-tRNA^{Gln} (0.0035 and 0.0014 s^{-1}, respectively; Table 2); this is in line with previous results archaeal GatCAB (10,13,14).

Deletion of the 3_{10} turn from *S. aureus* GatCAB resulted in a mutant enzyme that was 17-fold less efficient than wild-type mostly due to a difference in k_{cat} (Table 3), possibly due to the enzyme no longer recognizing the first base pair of the substrate aa-tRNA. However, consistent with our model, the removal of the 3_{10} turn from the *S. aureus* GatB resulted in a mutant *S. aureus* GatCAB that no longer strongly preferred tRNA substrates with a U1–A72 base pair to those with a G1–C72 base pair (Tables 2 and 3). For example the mutant *S. aureus* GatCAB could use the mutant *S. aureus* Glu-tRNA$^{Gln}_{GC}$ as a substrate about as well as wild-type *S. aureus* Glu-tRNA$^{Gln}_{UA}$ (0.03 and 0.05 s^{-1}, respectively, Table 2). In addition, the mutant *S. aureus* GatCAB could use *M. thermautotrophicus* Asp-tRNA^{Asn}, with its G1–C72 base pair, about as well as *Chlamydia trachomatis* Asp-tRNA^{Asn}, which has a U1–A72 base pair (Table 2) and was about as efficient in amidating *M. thermautotrophicus* Asp-tRNA$^{Asn}_{GC}$ as *S. aureus* Glu-tRNA$^{Gln}_{UA}$ (Table 3).

Consistent with our model, the insertion of the 3_{10} turn into *M. thermautotrophicus* GatCAB gave a mutant enzyme with preference for tRNA substrates with a U1–A72 base pair (Tables 2 and 3). The mutant *M. thermautotrophicus* GatCAB was about as efficient as wild-type *M. thermautotrophicus* GatCAB using *S. aureus*

Glu-tRNA$^{Gln}_{UA}$ as a substrate (Table 3). However, compared to wild-type *M. thermautotrophicus* GatCAB, the mutant enzyme was 10-fold less efficient with the *M. thermautotrophicus* Asp-tRNA$^{Asn}_{GC}$ substrate (Table 3). In addition, the mutant *M. thermautotrophicus* GatCAB preferred by 10-fold a substrate wild-type *S. aureus* Glu-tRNA$^{Gln}_{UA}$ substrate over the G1–C72 mutant Glu-tRNA^{Gln} (Table 2). Also, while wild-type *M. thermautotrophicus* GatCAB was nearly as active with *C. trachomatis* Asp-tRNA$^{Asn}_{UA}$ as with *M. thermautotrophicus* Asp-tRNA$^{Asn}_{GC}$, the insertion GatCAB mutant preferred *C. trachomatis* Asp-tRNA^{Asn}, which has a U1–A72 base pair (Table 2). These results indicate that insertion of the 3_{10} turn into GatB enables *M. thermautotrophicus* GatCAB to distinguish aa-tRNA with a U1–A72 base pair from ones with a G1–C72 base pair. Taken with the mutant *S. aureus* GatCAB data, these results strongly suggest that the 3_{10} turn in *S. aureus* GatCAB is crucial for distinguishing aa-tRNA with a U1–A72 from those with a G1–C72 base pair.

DISCUSSION

The bacterial GatCAB enzyme uses the first base pair of the acceptor stem and the tRNA D-loop for precise tRNA discrimination (11,13). Our results suggest that the U1–A72 base pair of tRNA^{Asn} and tRNA^{Gln} is recognized by a 3_{10} turn in the cradle domain of GatB, while the tail domain of GatB binds the D-loop.

The transamidosome is a ternary complex of *T. thermophilus* GatCAB, ND-AspRS and tRNA^{Asn} stable during the overall catalytic process (42). Such a structure would enable Asn-tRNA^{Asn} formation without the risk of free mischarged Asp-tRNA^{Asn} being used in protein synthesis. The complex would also protect the Asn-tRNA^{Asn} product from deacylation until it will be bound by EF-Tu and transported to the ribosome (42,43). Complexes between ND-GluRS, tRNA^{Gln}, and either Glu-AdT (GatCAB or GatDE) are also predicted to exist (12,42). Formation of these complexes between ND-aaRS, AdT and tRNA may explain why the AdTs recognize the specific identity elements in their tRNA substrates.

The structural models of the transamidosomes predict the ND-aaRS enzyme binds to the acceptor stem and anticodon loop of the tRNA (tRNA^{Gln} or tRNA^{Asn}) (12,42) (Supplementary Figure S7) in the same fashion as they do in the absence of AdT (44,45). This places the tRNA 3′-end into the synthetase active site to be aminoacylated; initially the first base pair of the tRNA's acceptor helix is not accessible to the 3_{10} turn of bacterial GatB in its role to discriminate tRNA isoacceptors. However, the tRNA's tertiary core (including the D-loop) is recognized (Supplementary Figure S7). Recognition of the D-loop by the AdT tail domain (11,12) may permit the amidotransferases to distinguish the ND-aaRS complexed with their tRNA transamidation substrates (tRNA^{Gln} or tRNA^{Asn}) from other tRNA isoacceptors (tRNA^{Glu} or tRNA^{Asp}) (12–14). For example, GatCAB recognition of the D-loop would enable the AdT to discriminate ND-AspRS bound to tRNA^{Asn} from the aaRS bound to tRNA^{Asp} despite the U1–A72 base pair being initially inaccessible to GatCAB. The variable loop of the tRNA in the transamidsome models is also accessible to the AdT, in particular the Lys rich motif in the tail domain of GatB, which may explain why archaeal GatCAB uses this element to discriminate tRNA^{Asn} from tRNA^{Asp} (13,14).

The transamidosome models (12,42) predict that after aminoacylation the tRNA's 3′ CCA terminus flips from active site in the ND-aaRS to the kinase active site of the AdT (42), similar to the tRNA movements seen in certain aaRSs with editing domains (46,47). In the case of the transamidosome, this movement enables the aminoacyl-moiety of the mischarged tRNA to be amidated by the AdT in the complex. Once the 3′ end of the acceptor stem flips from the aaRS active site into the transamidase active site of the AdT, the U1–A72 base pair may become accessible to the 3_{10} turn in bacterial GatB.

Recognition of the first base pair by bacterial GatCAB and the archaeal GatDE may be a proofreading step to ensure amidation of the mischarged tRNA substrate (Glu-tRNA^{Gln} and/or Asp-tRNA^{Asn}) and not the properly aminoacylated product of the ND-aaRS (Glu-tRNA^{Glu} or Asp-tRNA^{Asp}). Why this proofreading step is not required by the archaeal GatCAB is unclear, but presumably recognition of the tRNA tertiary core may be enough to ensure that GatCAB amidates Asp-tRNA^{Asn} and not Asp-tRNA^{Asp} (13,14).

It was speculated that the ancestor of GatB and GatE recognized the first base pair of its tRNA substrates (16). However, as the 3_{10} turn in the cradle domain of the *S. aureus* GatB for recognition of the U1–A72 base pair in tRNA^{Gln} is conserved only in bacterial GatB and not in archaeal GatB and GatE, this may not be the case. Instead, the common ancestor of GatB and GatE may not have recognized the first base pair of its tRNA substrate, with bacterial GatCAB and GatDE independently evolving to recognize the first base pair of tRNA. Thus, bacterial GatCAB and GatDE both recognizing the first base pair may have been a case of convergent and not divergent evolution.

ACCESSION NUMBERS

Coordinate and structure factor have been deposited in PDB with accession number 3IP4.

SUPPLEMENTARY DATA

Supplementary Data are available at NAR Online.

ACKNOWLEDGEMENTS

The authors are grateful to S. Chimnaronk, I. Heinemann, J. Ling and Y. Tanaka for many stimulating discussions, and to T. Tamura (National Institute of Advanced Industrial Science and Technology) for his gift of the *R. erythropolis* expression system. They thank the staff of SPring-8 BL41XU, 40B2 (2009A1119) and 45XU

beam lines for their help during collection of the X-ray data.

FUNDING

A.N. held a Research Fellowship of the Japan Society for the Promotion of Science for Young Scientists. Grants-in-Aid for Scientific Research (19370037 and 21370041 to M.Y.); Targeted Proteins Research Program (to I.T.) from the Ministry of Education, Culture, Sports, Science and Technology of Japan; Institute of General Medical Sciences and the US Department of Energy (to D.S.).

Conflict of interest statement. None declared.

REFERENCES

1. Ibba,M. and Söll,D. (2000) Aminoacyl-tRNA synthesis. *Annu. Rev. Biochem.*, **69**, 617–650.
2. Sheppard,K., Yuan,J., Hohn,M.J., Jester,B., Devine,K.M. and Söll,D. (2008) From one amino acid to another: tRNA-dependent amino acid biosynthesis. *Nucleic Acids Res.*, **36**, 1813–1825.
3. Lapointe,J., Duplain,L. and Proulx,M. (1986) A single glutamyl-tRNA synthetase aminoacylates $tRNA^{Glu}$ and $tRNA^{Gln}$ in *Bacillus subtilis* and efficiently misacylates *Escherichia coli* $tRNA^{Gln1}$ *in vitro*. *J. Bacteriol.*, **165**, 88–93.
4. Wilcox,M. and Nirenberg,M. (1968) Transfer RNA as a cofactor coupling amino acid synthesis with that of protein. *Proc. Natl Acad. Sci. USA*, **61**, 229–236.
5. Curnow,A.W., Ibba,M. and Söll,D. (1996) tRNA-dependent asparagine formation. *Nature*, **382**, 589–590.
6. Becker,H.D., Reinbolt,J., Kreutzer,R., Giegé,R. and Kern,D. (1997) Existence of two distinct aspartyl-tRNA synthetases in *Thermus thermophilus*. Structural and biochemical properties of the two enzymes. *Biochemistry*, **36**, 8785–8797.
7. Curnow,A.W., Hong,K., Yuan,R., Kim,S., Martins,O., Winkler,W., Henkin,T.M. and Söll,D. (1997) Glu-tRNAGln amidotransferase: a novel heterotrimeric enzyme required for correct decoding of glutamine codons during translation. *Proc. Natl Acad. Sci. USA*, **94**, 11819–11826.
8. Tumbula,D.L., Becker,H.D., Chang,W.Z. and Söll,D. (2000) Domain-specific recruitment of amide amino acids for protein synthesis. *Nature*, **407**, 106–110.
9. Roy,H., Becker,H.D., Reinbolt,J. and Kern,D. (2003) When contemporary aminoacyl-tRNA synthetases invent their cognate amino acid metabolism. *Proc. Natl Acad. Sci. USA*, **100**, 9837–9842.
10. Sheppard,K., Sherrer,R.L. and Söll,D. (2008) *Methanothermobacter thermautotrophicus* $tRNA^{Gln}$ confines the amidotransferase GatCAB to asparaginyl-tRNAAsn formation. *J. Mol. Biol.*, **377**, 845–853.
11. Nakamura,A., Yao,M., Chimnaronk,S., Sakai,N. and Tanaka,I. (2006) Ammonia channel couples glutaminase with transamidase reactions in GatCAB. *Science*, **312**, 1954–1958.
12. Oshikane,H., Sheppard,K., Fukai,S., Nakamura,Y., Ishitani,R., Numata,T., Sherrer,R.L., Feng,L., Schmitt,E., Panvert,M. *et al.* (2006) Structural basis of RNA-dependent recruitment of glutamine to the genetic code. *Science*, **312**, 1950–1954.
13. Bailly,M., Giannouli,S., Blaise,M., Stathopoulos,C., Kern,D. and Becker,H.D. (2006) A single tRNA base pair mediates bacterial tRNA-dependent biosynthesis of asparagine. *Nucleic Acids Res.*, **34**, 6083–6094.
14. Namgoong,S., Sheppard,K., Sherrer,R.L. and Söll,D. (2007) Co-evolution of the archaeal tRNA-dependent amidotransferase GatCAB with $tRNA^{Asn}$. *FEBS Lett.*, **581**, 309–314.
15. Deniziak,M., Sauter,C., Becker,H.D., Paulus,C.A., Giegé,R. and Kern,D. (2007) *Deinococcus* glutaminyl-tRNA synthetase is a chimer between proteins from an ancient and the modern pathways of aminoacyl-tRNA formation. *Nucleic Acids Res.*, **35**, 1421–1431.
16. Sheppard,K. and Söll,D. (2008) On the Evolution of the tRNA-dependent amidotransferases, GatCAB and GatDE. *J. Mol. Biol.*, **377**, 831–844.
17. Schmitt,E., Panvert,M., Blanquet,S. and Mechulam,Y. (2005) Structural basis for tRNA-dependent amidotransferase function. *Structure*, **13**, 1421–1433.
18. Wu,J., Bu,W., Sheppard,K., Kitabatake,M., Kwon,S.T., Söll,D. and Smith,J.L. (2009) Insights into tRNA-dependent amidotransferase evolution and catalysis from the structure of the *Aquifex aeolicus* enzyme. *J. Mol. Biol.*, **391**, 703–716.
19. Nakashima,N. and Tamura,T. (2004) A novel system for expressing recombinant proteins over a wide temperature range from 4 to 35 degrees C. *Biotechnol. Bioeng.*, **86**, 136–148.
20. Sheppard,K., Akochy,P.M., Salazar,J.C. and Söll,D. (2007) The *Helicobacter pylori* amidotransferase GatCAB is equally efficient in glutamine-dependent transamidation of Asp-tRNAAsn and Glu-tRNAGln. *J. Biol. Chem.*, **282**, 11866–11873.
21. Stura,E.A. (2000) Seeding techniques. In Ducroix,A. and Giegé,R. (eds), *Crystallization of Nucleic Acids and Proteins: A Practical Approach*, second edition. IRL Press, Oxford, pp. 177–207.
22. Otwinowski,Z. and Minor,W. (1997) Processing of X-ray Diffraction Data Collected in Oscillation Mode. In Carter,C.W.J. and Sweet,R.M. (eds), *Methods in Enzymology, Volume 276: Macromolecular Crystallography, part A*. Academic Press, New York, pp. 307–326.
23. Navaza,J. (1994) AMoRe: an automated package for molecular replacement. *Acta Crystallogr. Sect. A: Foundations Crystallogr.*, **50**, 157–163.
24. Yao,M., Zhou,Y. and Tanaka,I. (2006) LAFIRE: software for automating the refinement process of protein-structure analysis. *Acta Crystallogr. Sect. D: Biol. Crystallogr.*, **62**, 189–196.
25. Zyou,Y., Yao,M. and Tanaka,I. (2006) New algorithm for protein model building. *J. Appl. Crystallogr.*, **39**, 57–63.
26. Brünger,A.T., Adams,P.D., Clore,G.M., DeLano,W.L., Gros,P., Grosse-Kunstleve,R.W., Jiang,J.S., Kuszewski,J., Nilges,M., Pannu,N.S. *et al.* (1998) Crystallography & NMR system: A new software suite for macromolecular structure determination. *Acta Crystallogr. Sect. D: Biol. Crystallogr.*, **54**, 905–921.
27. Emsley,P. and Cowtan,K. (2004) Coot: model-building tools for molecular graphics. *Acta Crystallogr. Sect. D: Biol. Crystallogr.*, **60**, 2126–2132.
28. DeLano,W.L. (2002) The PyMOL Molecular Graphics System. *The PyMOL Molecular Graphics System*. DeLano Scientific, San Carlos, CA, USA.
29. Fujisawa,T., Inoue,K., Oka,T., Iwamoto,H., Uruga,T., Kumasaka,T., Inoko,Y., Yagi,N., Yamamoto,M. and Ueki,T. (2000) Small-angle X-ray scattering station at the SPring-8 RIKEN beamline. *J. Appl. Crystallogr.*, **33**, 797–800.
30. Konarev,P.V., Volkov,V.V., Sokolova,A.V., Koch,M.H.J. and Svergun,D.I. (2003) PRIMUS: a Windows PC-based system for small-angle scattering data analysis. *J. Appl. Crystallogr.*, **36**, 1277–1282.
31. Svergun,D.I. (1992) Determination of the regularization parameter in indirect-transform methods using perceptual criteria. *J. Appl. Crystallogr.*, **25**, 495–503.
32. Svergun,D.I., Barberato,C. and Koch,M.H.J. (1995) CRYSOL—a program to evaluate X-ray solution scattering of biological macromolecules from atomic coordinates. *J. Appl. Crystallogr.*, **28**, 768–773.
33. Leulliot,N., Chaillet,M., Durand,D., Ulryck,N., Blondeau,K. and van Tilbeurgh,H. (2008) Structure of the yeast tRNA m7G methylation complex. *Structure*, **16**, 52–61.
34. Boczkowska,M., Rebowski,G., Petoukhov,M.V., Hayes,D.B., Svergun,D.I. and Dominguez,R. (2008) X-ray scattering study of activated Arp2/3 complex with bound actin-WCA. *Structure*, **16**, 695–704.
35. Svergun,D.I. (1999) Restoring low resolution structure of biological macromolecules from solution scattering using simulated annealing. *Biophys. J.*, **76**, 2879–2886.
36. Volkov,V.V. and Svergun,D.I. (2003) Uniqueness of *ab initio* shape determination in small-angle scattering. *J. Appl. Crystallogr.*, **36**, 860–864.

37. Kozin,M.B. and Svergun,D.I. (2001) Automated matching of high- and low-resolution structural models. *J. Appl. Crystallogr.*, **34**, 33–41.
38. Sheppard,K., Akochy,P.M. and Söll,D. (2008) Assays for transfer RNA-dependent amino acid biosynthesis. *Methods*, **44**, 139–145.
39. Baick,J.W., Yoon,J.H., Namgoong,S., Söll,D., Kim,S.I., Eom,S.H. and Hong,K.W. (2004) Growth inhibition of *Escherichia coli* during heterologous expression of *Bacillus subtilis* glutamyl-tRNA synthetase that catalyzes the formation of mischarged glutamyl-tRNA1Gln. *J. Microbiol.*, **42**, 111–116.
40. Marck,C. and Grosjean,H. (2002) tRNomics: analysis of tRNA genes from 50 genomes of Eukarya, Archaea, and Bacteria reveals anticodon-sparing strategies and domain-specific features. *RNA*, **8**, 1189–1232.
41. Perona,J.J. and Hou,Y.M. (2007) Indirect readout of tRNA for aminoacylation. *Biochemistry*, **46**, 10419–10432.
42. Bailly,M., Blaise,M., Lorber,B., Becker,H.D. and Kern,D. (2007) The transamidosome: a dynamic ribonucleoprotein particle dedicated to prokaryotic tRNA-dependent asparagine biosynthesis. *Mol. Cell*, **28**, 228–239.
43. Huot,J.L., Balg,C., Jahn,D., Moser,J., Émond,A., Blais,S.P., Chênevert,R. and Lapointe,J. (2007) Mechanism of a GatCAB amidotransferase: aspartyl-tRNA synthetase increases its affinity for Asp-tRNAAsn and novel aminoacyl-tRNA analogues are competitive inhibitors. *Biochemistry*, **46**, 13190–13198.
44. Ruff,M., Krishnaswamy,S., Boeglin,M., Poterszman,A., Mitschler,A., Podjarny,A., Rees,B., Thierry,J.C. and Moras,D. (1991) Class II aminoacyl transfer RNA synthetases: crystal structure of yeast aspartyl-tRNA synthetase complexed with $tRNA^{Asp}$. *Science*, **252**, 1682–1689.
45. Sekine,S., Nureki,O., Shimada,A., Vassylyev,D.G. and Yokoyama,S. (2001) Structural basis for anticodon recognition by discriminating glutamyl-tRNA synthetase. *Nat. Struct. Biol.*, **8**, 203–206.
46. Nureki,O., Vassylyev,D.G., Tateno,M., Shimada,A., Nakama,T., Fukai,S., Konno,M., Hendrickson,T.L., Schimmel,P. and Yokoyama,S. (1998) Enzyme structure with two catalytic sites for double-sieve selection of substrate. *Science*, **280**, 578–582.
47. Silvian,L.F., Wang,J. and Steitz,T.A. (1999) Insights into editing from an Ile-tRNA synthetase structure with $tRNA^{Ile}$ and mupirocin. *Science*, **285**, 1074–1077.